1134 *Chem. Mater.* **2010,** *22,* 1134–1141
DOI:10.1021/cm902425k

CHEMISTRY OF MATERIALS
Article

Performance and Characterization of (La, Sr)MnO_3/YSZ and $La_{0.6}Sr_{0.4}Co_{0.2}Fe_{0.8}O_3$ Electrodes for Solid Oxide Electrolysis Cells†

Miguel A. Laguna-Bercero, John A. Kilner, and Stephen J. Skinner*

Department of Materials, Imperial College London, SW7 2AZ London, United Kingdom

Received August 6, 2009. Revised Manuscript Received November 16, 2009

Two alternative oxygen electrodes (anodes), $La_{0.6}Sr_{0.4}Co_{0.2}Fe_{0.8}O_{3-\delta}$ (LSCF) and $La_{0.8}Sr_{0.2}MnO_{3-\delta}$ (lanthanum strontium manganite)/YSZ (yttria stabilized zirconia), were tested in 10Sc1CeSZ (scandia and ceria stabilized zirconia) based electrolysis cells and electrochemically evaluated. In all the samples, the impedance response at OCV is characterized by a small arc at high frequencies around 10 kHz assigned to the Ni/YSZ polarization and a larger arc at low frequencies at about 200 Hz associated with the oxygen electrode. Lower polarization resistances were found for the LSCF electrode. Good performance in electrolysis mode was measured at an operating temperature of 800 °C and using 70% H_2O at the Ni/YSZ cathode. Area specific resistance (ASR) values of 0.93 and 0.79 $\Omega.cm^2$ were obtained for the LSM/YSZ and the LSCF samples respectively. After operation, we have observed a ~10% increase in the ohmic resistance for the LSM/YSZ sample. This degradation was studied by both X-ray diffraction and scanning electron microscopy. LSM/YSZ and LSCF are suggested as good candidates for oxygen electrodes in high temperature electrolysis cells. Finally, good electrochemical performance was also observed in reversible fuel cell mode.

1. Introduction

The prospect of a hydrogen economy will require the development of clean and efficient methods for the production of hydrogen. At present, most hydrogen is produced by the steam reforming of methane, with the consequent problem of carbon emissions to the atmosphere. Other cleaner methods are required, such as biomass, water electrolysis, biological systems, and the use of thermochemical cycles. Electrolysis of water is probably currently the most advanced clean technology, as it is widely developed for use at low temperature using alkaline electrolyzers. As an alternative, high-temperature solid oxide electrolyzers (SOE) are particularly favorable as they present kinetic and thermodynamic advantages because of their elevated temperature of operation. The electrical energy demand decreases when increasing the temperature, and in addition, overvoltages at both anode and cathode are reduced. The electrochemical reactions that occur in a SOE are the inverse reactions to those in a solid oxide fuel cell (SOFC), and the polarization of the cell is then the opposite of that in a SOFC. In a SOE, water is supplied to the cathode side of the cell (anode electrode in SOFC mode) as a reactant. Oxygen ions are transported to the anode through the electrolyte, and hydrogen is produced at the cathode side. These devices can then operate reversibly, producing hydrogen from steam (SOE mode), and then using the stored hydrogen to generate electricity and heat (SOFC mode), acting as a storage device for electrical energy.

For example, nuclear power, renewable energy, and waste heat from high-temperature industrial processes could all be used to supply the heat and power needed for electrolysis. The use of nuclear energy combined with a solid oxide fuel cell (SOFC) operating in the reverse direction of current flow to split steam is being investigated and the results are very promising.[1,2] SOEs are also capable of electrolyzing carbon dioxide to carbon monoxide ($CO_2 \rightarrow CO + 1/2O_2$), as has been recently demonstrated.[3] Co-electrolysis of steam and CO_2 is also possible in a SOE, yielding synthesis gas ($CO + H_2$) that can be catalyzed to various types of synthetic fuels.[4] Another possibility for SOEs is natural gas-assisted electrolysis, using partial ($CH_4 \rightarrow CO + H_2$) or total oxidation ($CH_4 \rightarrow CO_2 + H_2O$).[5] Thus, SOEs offer a wide range of possible applications; however, most recent work has focused on steam electrolysis.

Initial development of SOEs was reported in the 1980s with the Hot Elly (high operating temperature electrolysis) system developed by Dornier GmbH[6] and

†Accepted as part of the 2010 "Materials Chemistry of Energy Conversion Special Issue".

*Corresponding author. E-mail: s.skinner@imperial.ac.uk.

(1) Herring, J. S.; O'Brien, J. E.; Stoots, C. M.; Hawkes, G. L.; Hartvigsen, J. J.; Shahnam, M. *Int. J. Hydrogen Energy* **2007**, *32*, 440.
(2) Fujiwara, S.; Kasai, S.; Yamauchi, H.; Yamada, K.; Makino, S.; Matsunaga, K.; Yoshino, M.; Kameda, T.; Ogawa, T.; Momma, S.; Hoashi, E. *Prog. Nucl. Energy* **2008**, *5*, 422.
(3) Ebbesen, S. D.; Mogensen, M. *J. Power Sources*. **2009**, *193*, 349.
(4) Chorkendorff I.; Niemantsverdriet, J. W. *Concepts of Modern Catalysis and Kinetics*; Wiley-VCH, Weinheim, Germany, 2006.
(5) Martínez-Frías, J.; Pham, A. Q.; Aceves, S. M *Int. J. Hydrogen Energy* **2003**, *28*, 483.
(6) Quandt, K. H.; Streicher, R. *Int. J. Hydrogen Energy* **1986**, *11*, 309.

 Published on Web 12/08/2009

Scheme 1. Schematic Representation of the Experimental Setup Employed for the Electrolysis Experiments[a]

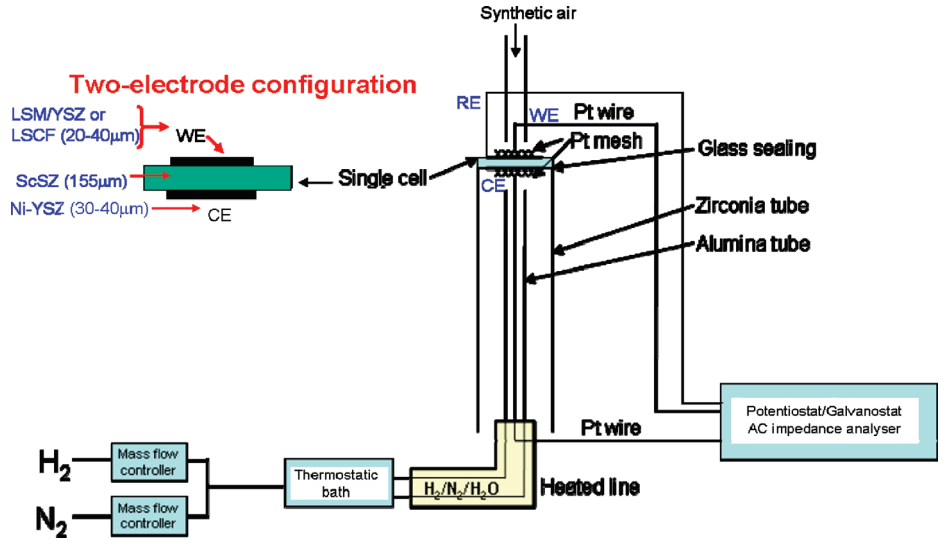

[a] The reference electrode indicated was used in AC impedance measurements to attempt to distinguish anode and cathode contributions. All electrolysis measurements were performed in two-electrode mode.

the Westinghouse program with a tubular design.[7] In the past few years, this field has attracted many research groups and the results suggest that this technology is much more efficient than low-temperature alkaline electrolyzers. Several efforts have also been made in order to improve the durability of the cells and to optimize the performance of the electrodes.[1,8−15]

$La_{1-x}Sr_xCo_yFe_{1-y}O_{3-\delta}$ (LSCF)-doped perovskites based on $LaCoO_3$ and composite electrodes made of a perovskite and a solid electrolyte such as the $La_{1-x}Sr_x$-$MnO_{3-\delta}$ (LSM)/$Y_xZr_{1-x}O_{2-\delta}$ (YSZ) have been proposed as an alternative to the conventional LSM for oxygen electrodes in both SOFCs and electrolyzers.[16,17] These materials present high electronic conductivity, high oxygen ion conductivity, and thus a high oxygen surface exchange coefficient for fast kinetics at the gas/cathode interface. A further advantage of these materials is that they typically display mixed ionic and electronic conduction (MIEC) and are therefore excellent candidates for SOE electrodes. A further point is that there is good evidence of a positive correlation between the performance of air electrodes in both SOFC and SOE modes.[12,18]

However, there are contradictions in the literature about the performance, in particular, of LSM/YSZ in SOE mode. Some authors have reported that LSM/YSZ electrodes show poor performance under electrolysis conditions.[11,19] Wang et al.[11] concluded that the enhancement associated with cathodic polarization is lost during electrolysis. On the contrary, the best results in SOE cells to date were reported by Jensen et al.[20] using LSM/YSZ composite oxygen electrodes. It is not currently clear why such differences exist, as our knowledge of high temperature electrolysis is limited. Therefore, in an attempt to identify an anode with good electrochemical performance in electrolysis mode and to address some of these contradictions, we report our analysis of electrochemical cells after combined SOFC-SOE experiments, in terms of the structural, microstructural and electrical characterization for both LSM/YSZ and LSCF perovskite-based electrodes. Mechanisms of the oxygen reduction and evolution reaction for both electrode types will be discussed.

2. Experimental Procedures

Ni/YSZ (electrode)-10Sc1CeSZ (electrolyte) half-cells provided by Kerafol GmbH, Germany, were used for the electrochemical experiments. The pellets consisted of 10% Sc_2O_3−1% CeO_2−ZrO_2 (10Sc1CeSZ) electrolyte (mol %) of 20 mm diameter and 155 ± 5 μm thickness, and NiO/8% Y_2O_3−ZrO_2 (YSZ) electrode (mol %) of about 40 μm thickness. Two compositions of oxygen electrode were tested. The first electrode was composed of $La_{0.6}Sr_{0.4}Co_{0.2}Fe_{0.8}O_{3-\delta}$ (LSCF) powder (99.9%, Praxair, USA) and a commercial ink vehicle (Fuelcell Materials, USA) triple-roll-milled together to prepare an electrode ink. LSCF powder was previously ball-milled in acetone for 48 h to reduce the particle size. A second electrode of $La_{0.8}Sr_{0.2}MnO_{3-\delta}$ (lanthanum strontium manganite)/YSZ ink (50/50 wt %) (Fuelcell Materials, USA) was similarly prepared with the same commercial ink vehicle. Those

(7) Maskalick, N. J. *Int. J. Hydrogen Energy* **1986**, *11*, 563.
(8) Hauch, A.; Ebbesen, S. D.; Jensen, S. H.; Mogensen, M. *J. Mater. Chem.* **2008**, *18*, 2331.
(9) Yang, X.; Irvine, J. T. S. *J. Mater. Chem.* **2008**, *18*, 2349.
(10) Laguna-Bercero, M. A.; Skinner, S. J.; Kilner, J. A. *J. Power Sources* **2009**, *192*, 126.
(11) Wang, W.; Huang, Y.; Jung, S.; Vohs, J. M.; Gorte, R. J. *J. Electrochem. Soc.* **2006**, *153*, A2066.
(12) Marina, O. A.; Pederson, L. R.; Williams, M. C.; Coffey, G. W.; Meinhardt, K. D.; Nguyen, C. D.; Thomsen, E. C. *J. Electrochem. Soc.* **2007**, *154*, B452.
(13) Schiller, G.; Ansar, A.; Lang, M.; Patz, O. *J. Appl. Electrochem.* **2009**, *39*, 293.
(14) Brisse, A.; Schefold, J.; Zahid, M. *Int. J. Hydrogen Energy* **2008**, *33*, 5375.
(15) Elangovan, S.; Hartvigsen, J. J. *Int. J. Appl. Ceram. Technol.* **2007**, *4*, 109.
(16) Jiang, S. P. *J. Mater. Sci.* **2008**, *43*, 6799.
(17) Sunarso, J.; Baumann, S.; Serra, J. M.; Meulenberg, W. A.; Liu, S.; Lin, Y. S.; Diniz da Costa, J. C. *J. Membr. Sci.* **2008**, *320*, 13.
(18) Hauch, A.; Jensen, S. H.; Mogensen, M.; Ramousse, S. *J. Electrochem. Soc.* **2006**, *153*, A1741.
(19) Chen, X. J.; Chan, S. H.; Khor, K. A. *Electrochem. Solid-State Lett.* **2004**, *7*, A144.
(20) Jensen, S. H.; Larsen, P. H.; Mogensen, M. *Int. J. Hydrogen Energy* **2007**, *32*, 3253.

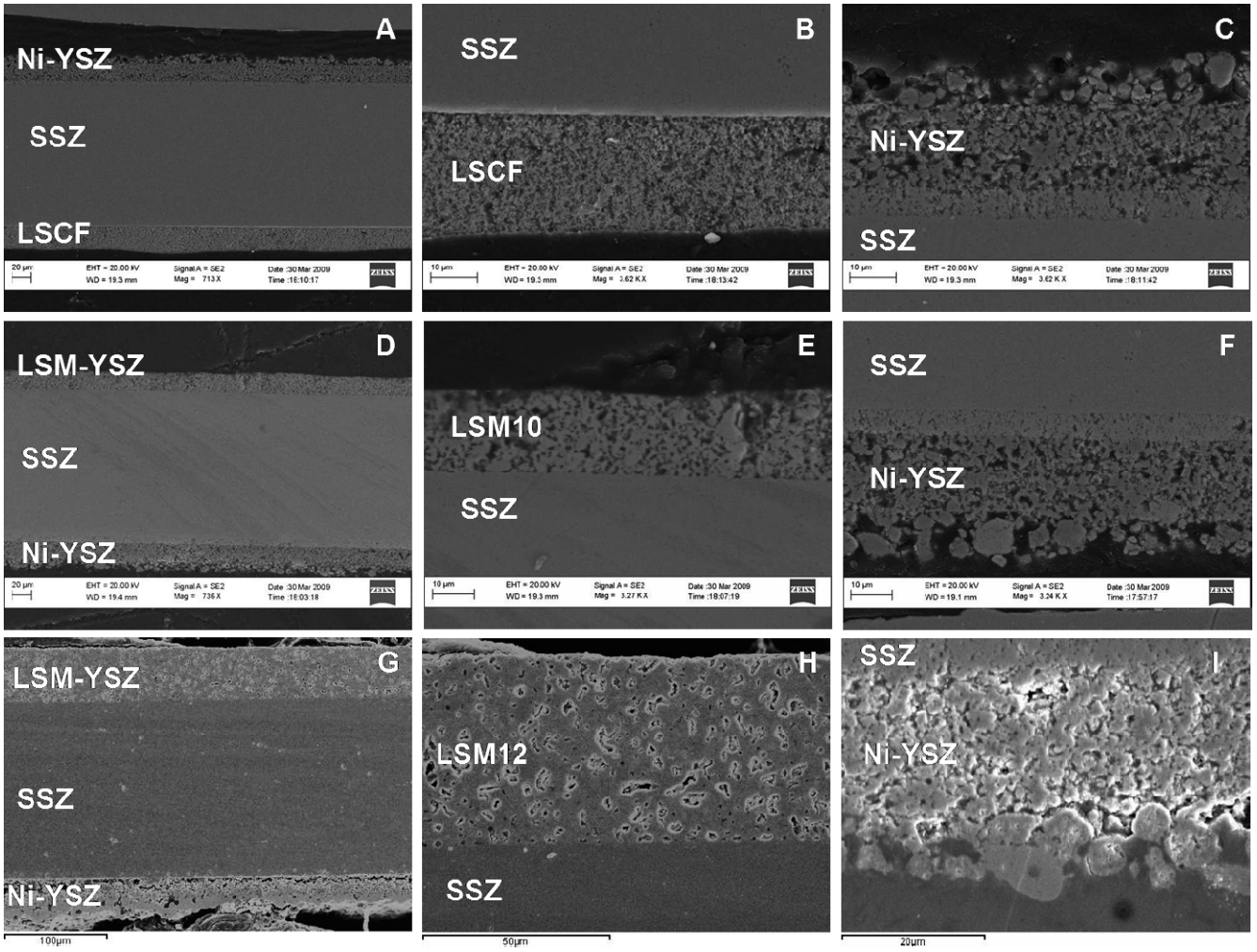

Figure 1. SEM micrographs (polished cross-sections) of tested single cells. (A) Ni/YSZ-10Sc1CeSZ-LSCF cell (LSCF10); (B) LSCF-10Sc1CeSZ and (C) Ni/YSZ-10Sc1CeSZ interfaces of the LSCF10 cell; (D) Ni/YSZ-10Sc1CeSZ-LSM/YSZ cell (LSM10); (E) LSM/YSZ-10Sc1CeSZ and (F) Ni/YSZ-10Sc1CeSZ interfaces of the LSM10 cell; (G) Ni/YSZ-10Sc1CeSZ- LSM/YSZ cell (LSM12); (H) LSM/YSZ-10Sc1CeSZ and (I) Ni/YSZ-10Sc1CeSZ interfaces of the LSM12 cell.

inks were then deposited on the half cells by screen-printing, dried in air at 100 °C, and then sintered in air at temperatures of between 1050 and 1250 °C.

The phase purity of each of the samples was verified by X-ray powder diffraction (XRD) using a Philips PW1700 series diffractometer with Cu Kα radiation. Scanning Electron Microscopy (SEM) was performed under an accelerating voltage of 20 kV using a LEO FE-SEM and a JEOL 840A SEM (JEOL, USA) fitted with Oxford Instruments INCA energy dispersive analytical system (EDS) for elemental X-ray analysis.

The experimental setup for the fuel cell/electrolysis measurements is described in Scheme 1. A two-electrode configuration was used in all cases. Pt wires were used for the current supply and potential probe and a Pt mesh was used at each electrode as a current collector. The sample was then attached to a zirconia tube and sealed using a glass sealant (Encapsulant 8190, DuPont). Mixtures of hydrogen/nitrogen were supplied to the cathode in order to avoid oxidation of Ni to NiO. Steam was supplied to the cathode by the use of a gas bubbler in water surrounded by a thermostatic bath maintained at a constant temperature for the required amount of steam with the steam content measured using a humidity sensor. All gas lines located downstream of the humidifier were externally heated in order to prevent steam condensation. The anode side of the cell was exposed to laboratory air.

Galvanostatic, galvanodynamic, and electrochemical impedance spectroscopy (EIS) experiments were performed using an Autolab PGSTAT30 fitted with a frequency response analyzer (FRA) (Autolab, EcoChemie, Netherlands). Impedance measurements under potential load were performed in potentiostatic mode using a sinusoidal signal amplitude of 50 mV over the frequency range of 10 kHz to 0.1 Hz. A reference electrode, as described by Liu et al.,[21] was only used in AC impedance experiments in order to try to distinguish anode and cathode contributions and not in the electrolysis measurements.

3. Results and Discussion

Microstructural Analysis. Four alternative oxygen electrodes were tested on samples using Ni/YSZ-10Sc1CeSZ substrates: (i) LSM/YSZ sintered at 1050 °C (LSM10); (ii) LSM/YSZ sintered at 1200 °C (LSM12); (iii) $La_{0.6}Sr_{0.4}Co_{0.2}F_{0.8}O_3$ sintered at 1050 °C (LSCF); and (iv) Pt electrode sintered at 900 °C (Pt). All samples were sintered for a period of 1 h. Typical microstructures for the LSCF10, LSM10, and LSM12 samples are presented in Figure 1. 10Sc1CeSZ electrolytes

(21) Liu, J.; Co, A. C.; Paulson, S.; Birss, V. I. *Solid State Ionics* **2006**, *177*, 377.

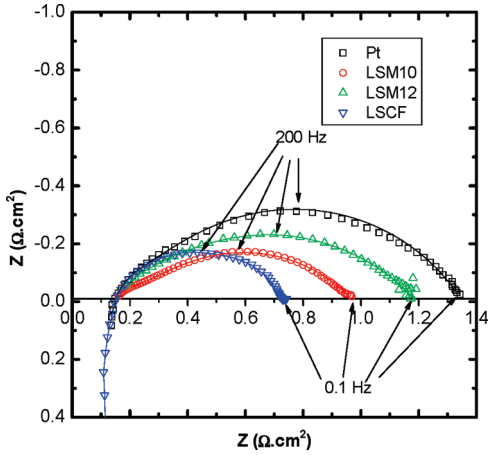

Figure 2. AC impedance measurements recorded at OCV and 800 °C for different single cells under 70% H_2O/ 24% N_2/ 6%H_2. Symbols correspond to the experimental data and solid lines correspond to fitted results using equivalent circuits.

(~155 μm thick) present a fully dense microstructure for all samples (as seen in micrographs A, D, and G for the LSCF10, LSM10, and LSM12 samples, respectively). The Ni/YSZ electrodes are also identical for all samples. Their microstructures consist of an anode functional layer (AFL) of 5 μm thickness and a support of about 25−30 μm thickness acting as a current collector, as seen in micrographs C, F, and I for the LSCF, LSM10, and LSM12 samples, respectively. Approximated thicknesses of the oxygen electrodes are 25, 20, and 40 μm for the LSCF (micrograph B), LSM10 (E), and LSM12 (H), respectively. Good adhesion is observed in all of the electrode−electrolyte interfaces: LSCF-10Sc1CeSZ (B), LSM10−10Sc1CeSZ (E), LSM12−10Sc1CeSZ (H), and Ni/YSZ-10Sc1CeSZ (C, F, and I) respectively. LSCF (B) and LSM10 (E) present a homogeneous distribution of pores and particles in order to obtain optimum gas and electronic transport as well as good thermomechanical stability with the 10Sc1CeSZ electrolyte. The microstructure of the LSM12 electrode (H) indicates a higher density and thus is expected to have better adhesion with the electrolyte.

Finally, EDS microanalysis and mapping were performed on all of the interfaces in order to detect any impurities or secondary phases, such as the undesired insulating lanthanum (or strontium) zirconante ($La_2Zr_2O_7$). We have found no evidence of reactivity between the electrodes and the electrolyte.

Electrical Characterization. Electrolysis experiments were performed as a function of temperature for each of the cells. The gas compositions used were pH_2O = 0.7 atm, pN_2 = 0.24 atm, pH_2 = 0.06 atm for the cathode side (Ni/YSZ) and laboratory air for the oxygen electrode side. Prior to the electrolysis experiments, EIS data were recorded at open circuit voltage (OCV).

Figure 2 shows the initial impedance response, in air, for the different samples using two-electrode configuration. The ohmic resistance for all samples was measured to be ~ 0.16 Ω cm^2, as expected for 155 μm 10Sc1CeSZ electrolyte resistance and also in concordance with similar electrolyte-supported cells in the literature.[22] An inductive loop is usually observed at low frequencies and can be attributed to the activation of a passive layer at the electrode surface.[23] As seen in Figure 2, polarization resistance of the electrodes decreased according to Pt > LSM12 > LSM10 > LSCF.

Scheme 2. Schematic Representation of the Equivalent Circuit Employed to Fit the Impedance Data

Equivalent circuits were used to fit the electrical data. The analysis of the Nyquist diagrams is extremely complex.[24,25] Impedance spectra of LSCF electrodes correspond to at least two overlapping depressed arcs, one associated with bulk or surface diffusion and the other associated with surface exchange of oxygen and charge transfer.[26,27] Electrocatalytic activity is also strongly affected by the microstructure, as it determines the kinetics of the oxygen surface exchange and the region where oxygen reduction takes place. Bebelis et al.[28] studied the electrocatalytic performance of different compositions of LSCF electrodes as well as LSM/YSZ composites. They found that LSCF presents higher electrocatalytic activity than the LSM/YSZ electrode interfaced to gadolinia doped ceria (GDC). Analysis of LSM/YSZ composite electrodes is also complex, and there is some disagreement over the mechanism and kinetics for O_2 reduction. For example, Jørgensen et al.[29] found from impedance experiments that there are at least five processes in the oxygen reduction reaction. Kim et al.[30] found that the O_2 reduction reaction is limited by the transfer and surface diffusion of oxygen ions. On the contrary, Murray et al.[31] concluded that the reaction is limited by oxygen adsorption and dissociation. Finally, Zhen et al.[32] studied different contents in the LSM/YSZ composites. They found that when increasing the YSZ content in the composite, there is a transition from the dominant electronic conducting LSM electrode to a MIEC behavior, similar to that of the LSCF. The addition of YSZ enhances the number of triple phase boundaries (TPBs) and also promotes the surface exchange processes for the O_2 reduction reaction on the LSM/YSZ composite electrodes.

(22) Mosch, S; Trofimenko, N.; Kusnezoff, M.; Betz, T.; Kellner, M. *Solid State Ionics* **2008**, *179*, 1606.
(23) McDonald, J. R. *Impedance Spectroscopy*; New York: Wiley, 1987.
(24) Alder, S. B.; Lane, J. A.; Steele, B. C. H. *J. Electrochem. Soc.* **1996**, *143*, 3554.
(25) Esquirol, A.; Brandon, N. P.; Kilner, J. A.; Mogensen, M. *J. Electrochem. Soc.* **2004**, *151*, A1847.
(26) Dusastre, V.; Kilner, J. A. *Solid State Ionics* **1999**, *126*, 163.
(27) Perry Murray, E.; Sever, M. J.; Barnett, S. A. *Solid State Ion.* **2002**, *148*, 27.
(28) Bebelis, S.; Kotsionopoulos, N.; Mai, A.; Tietz, F. *J. Appl. Electrochem.* **2007**, *37*, 15.
(29) Jørgensen, M. J.; Mogensen, M. *J. Electrochem. Soc.* **2001**, *152*, A1433.
(30) Kim, J. D.; Kim, G. D.; Moon, J. W.; Park, Y. i.; Lee, W. H.; Kobayashi, K.; Nagai, M.; Kim, C. E. *Solid State Ionics* **2001**, *143*, 379.
(31) Perry Murray, E.; Tsai, T.; Barnett, S. A. *Solid State Ionics* **1998**, *110*, 235.
(32) Zhen, Z. D.; Jiang, S. P. *J. Electrochem. Soc.* **2006**, *153*, A2245.

Table 1. Impedance Parameters Obtained for the Four Electrodes Analyzed by Fitting of the Experimental Data Obtained at 800 °C

sample	R_e (Ω cm^2)	R_1 (Ω cm^2)	CPE1 ($\times 10^{-3}$) $Q((Fs)^{1-n}/cm^2)$	CPE1 n	R_2 (Ω cm^2)	CPE2 ($\times 10^{-3}$) $Q((Fs)^{1-n}/cm^2)$	CPE2 n
Pt	0.155(3)	0.089(5)	0.87(6)	0.86(3)	1.15(2)	9.3(4)	0.640(9)
LSM12	0.158(2)	0.064(4)	1.8(8)	0.89(4)	0.988(6)	10.8(5)	0.552(3)
LSM10	0.159(8)	0.067(4)	1.7(2)	0.83(4)	0.776(4)	10.7(2)	0.588(4)
LSCF	0.152(5)	0.078(6)	1.2(2)	0.87(5)	0.582(6)	14.3(7)	0.630(9)

Analysis of Ni/YSZ electrodes also presents some difficulties and different interpretations are found in the literature.[33] Up to four different processes have been found in the impedance spectra, associated with adsorption and diffusion on the electrode, charge transfer reaction, and ionic transport in YSZ.[34−38]

Analysis of the impedance spectra for single cells is usually more complex, as we have to analyze both anode and cathode in the same spectra. As seen in Figure 2, in all the samples the impedance response at OCV is usually characterized by a small arc at high frequencies at around 10 kHz and a larger arc at low frequencies at about 200 Hz. Probably, more than two different electrode processes exist (as discussed previously up to four or five different processes have been reported for each electrode), but in these experiments we are not able to distinguish more than two processes. The impedance spectra plotted in Figure 2 were analyzed by fitting the data with the equivalent circuit shown in Scheme 2. In this scheme, L corresponds to an inductance, which is usually associated with the platinum current/voltage probes, or to the high-frequency phase shift of the electrochemical equipment; R_e is the ohmic resistance of the electrolyte; (R_1, CPE1) and (R_2, CPE2) correspond to the high- and low-frequency arcs, respectively. The values obtained from the equivalent circuit fitting are shown in Table 1.

Capacitance values (C) and relaxation frequencies (f) for each contribution are calculated according to eqs 1 and 2, respectively.[39] The obtained values are shown in table 2, as well as the total area specific resistance ($ASR_{total} = R_e + R_1 + R_2$).

$$C = (R^{1-n}Q)^{1/n} \quad (1)$$

$$f = \frac{(RQ)^{-1/n}}{2\pi} \quad (2)$$

From Table 1, we observe that all R_1 values are similar for the different samples ($\sim$0.07 Ω cm^2) and much smaller than R_2. It is also well-known that usually the contribution from anode polarization is much smaller than that of the cathode and thus electrode resistance of the cell

Table 2. Impedance Parameters (C, f, and ASR_{total}) for the Four Electrode Compositions Recorded at 800 °C

sample	C1 (F cm^{-2})	f1 (Hz)	C2 (F cm^{-2})	f2 (Hz)	ASR_{total} (Ω cm^2)
Pt	1.86×10^{-4}	9597	7.24×10^{-4}	191	1.39(1)
LSM12	2.96×10^{-4}	8391	2.71×10^{-4}	594	1.21(1)
LSM10	2.65×10^{-4}	8974	3.73×10^{-4}	550	1.00(2)
LSCF	3.00×10^{-4}	6800	8.59×10^{-4}	318	0.81(2)

is mainly due to cathode polarization,[40] suggesting that R_1 could be associated with the Ni/YSZ electrode. To confirm this, we performed experiments using a reference electrode. Although the reference electrode was placed about 20 electrolyte thicknesses away from the active electrodes to avoid potential gradients along the electrolyte surface, we were not able to obtain meaningful results possibly due to a small misalignment of the electrodes.[41] The use of the three-electrode configuration reported by Offer et al.[42] will be used to resolve this issue in future experiments. Finally, experiments as a function of the steam concentration supplied to the Ni-YSZ electrode were also carried out and we have observed that R_1 response increases when decreasing the steam concentration. According to this evidence, we can then assign R_1 to the Ni/YSZ electrode. As observed in Table 2, the calculated values of capacitance and peak frequencies are around $(2-3) \times 10^{-4}$ F cm^{-2} and 7−9 kHz, respectively. These results are in good agreement with the high frequency arc observed by Jiang et al.,[36] which they associate with charge transfer in the electrode. They also observe a smaller arc at lower frequencies associated with H_2 adsorption and diffusion, which we do not distinguish and could be hidden with the oxygen electrode contribution.

R_2 is then assigned in all samples to the different oxygen electrodes. As we can observe in table 1, R_2 values decrease according to: Pt > LSM12 > LSM10 > LSCF. Some differences were found for the polarization resistances of the same material (LSM/YSZ) sintered at different temperatures. The higher polarization resistance of the LSM12 sample (sintered at 1200 °C) in comparison with LSM10 (sintered at 1050 °C) is attributed to the denser microstructure, as observed in Figure 1. As reported by Tanner et al.,[43] gas phase diffusion in porous composite electrodes is expected to be a rate-determining step at porosities lower than 20%, resultin in a significant increase in gas-phase diffusion. From these results we can conclude that LSCF is a suitable candidate for the oxygen electrode in both SOFC and SOE mode. LSM10

(33) Gewies, S; Bessler, W. G. *J. Electrochem. Soc.* **2008**, *155*, B937.
(34) Primdahl, S.; Mogensen, M. *J. Electrochem. Soc.* **1997**, *144*, 3409.
(35) Holtappels, P.; Vinke, I. C.; de Haart, L. G. J.; Stimming, U. *J. Electrochem. Soc.* **1999**, *146*, 2976.
(36) Jiang, S. P.; Badwal, S. P. S. *Solid State Ionics* **1999**, *123*, 209.
(37) Matsuzaki, Y.; Yasuda, I. *J. Electrochem. Soc.* **2000**, *147*, 475.
(38) Sonn, V.; Leonide, A.; Ivers-Tiffée, E. *J. Electrochem. Soc.* **2008**, *155*, B675.
(39) Fleig, J. *Solid State Ionics* **2002**, *150*, 181.
(40) *High Temperature Solid Oxide Fuel Cells: Fundamentals, Designs and Applications*; Singhal, S.C., Kendall, K., Eds.; Elsevier: Oxford, U.K., 2003.
(41) Adler, S. B.; Henderson, B. T; Wilson, M. A.; Taylor, D. M.; Richards, R. E. *Solid State Ionics* **2000**, *134*, 35.
(42) Offer, G. J.; Shearing, P.; Golbert, J. I.; Brett, D. J. L.; Atkinson, A.; Brandon, N. P. *Electrochim. Acta* **2008**, *53*, 7614.
(43) Tanner, C. W.; Fung, K. Z.; Virkar, A. V. *J. Electrochem. Soc.* **1997**, *144*, 121.

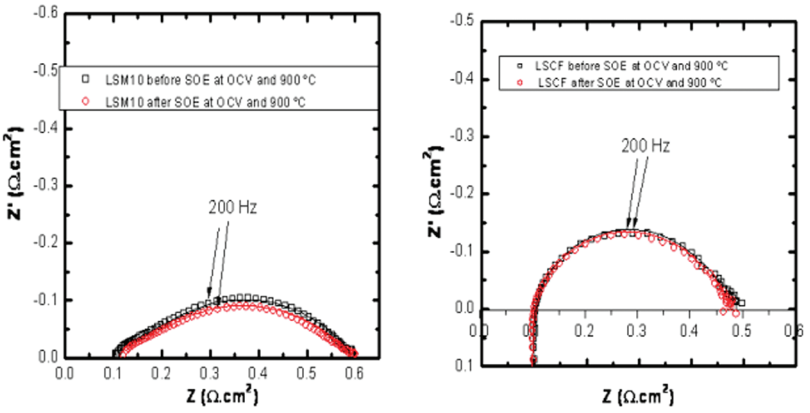

Figure 3. AC impedance measurements recorded at OCV and 900 °C for the LSM10 (left) and LSCF (right) samples before and after SOFC-SOE experiments under 70% H_2O/ 24% N_2/ 6%H_2. Symbols correspond to the experimental data and lines correspond to fitted results using equivalent circuits.

Table 3. Impedance Parameters for the LSM10 and LSCF Samples Obtained by Fitting the Experimental Data Obtained at 900 °C Both before and after Electrolysis

sample	R_e (Ω cm^2)	R_1 (Ω cm^2)	CPE1 ($\times 10^{-3}$) Q((Fs)$^{1-n}$/cm^2)	CPE1 n	R_2 (Ω cm^2)	CPE2 ($\times 10^{-3}$) Q((Fs)$^{1-n}$/cm^2)	CPE2 n
LSM10 before	0.107(3)	0.055(3)	4.1(5)	0.80(3)	0.448(8)	45(2)	0.598(8)
LSM10 after	0.124(4)	0.069(9)	2.8(1)	0.78(4)	0.442(5)	50(1)	0.536(4)
LSCF before	0.0976(5)	0.052(4)	5.2(6)	0.79(2)	0.34(1)	6.7(5)	0.84(1)
LSCF after	0.0967(4)	0.054(2)	6.6(4)	0.76(3)	0.34(1)	8.6(3)	0.80(2)

Table 4. Impedance Parameters (C and ASR_{total}) for the LSM10 and LSCF Samples Both before and after Electrolysis

sample	C1 (F cm^{-2})	C2 (F cm^{-2})	ASR_{total} (Ω cm^2)
LSM10 before	5.02×10^{-4}	0.0033	0.61(1)
LSM10 after	2.51×10^{-4}	0.0018	0.63(1)
LSCF before	5.85×10^{-4}	0.0021	0.49(2)
LSCF after	5.38×10^{-4}	0.002	0.49(2)

also presents an optimized microstructure and is another good candidate for SOFC and SOE applications.

SOFC-SOE galvanostatic experiments were also performed for both samples. For example, in SOE mode at 800 °C and using 70% H_2O at the Ni-YSZ electrode, ASR values of 0.93 and 0.79 Ω cm^2 were obtained for the LSM10 and the LSCF samples respectively. Under SOFC mode, ASR values decrease to 0.83 and 0.70 Ω cm^2 for the LSM10 and the LSCF samples, respectively. The nonlinearity of the cell response under anodic and cathodic polarization at temperatures up to 800 °C is explained in detail in ref 44. Both LSM10 and LSCF samples become fully reversible at 850 °C. All ASR values were obtained from the slope of the IV curves and are also in concordance with the impedance values reported. The good performance of the LSM10 sample is in agreement with the results of Jensen et al.[20] using LSM/YSZ composite oxygen electrodes, but also contradicts refs 11 and 19, as discussed in the introduction. Recently, Backhaus-Ricoult et al.[45] studied the surface chemistry of LSM/YSZ composites under polarization. They observed that there is a strong enrichment of the YSZ surface in Mn^{2+} that provides high electronic conductivity in the zirconia

(44) Laguna-Bercero, M. A.; Kilner, J. A.; Skinner, S. J. Solid State Ionics **2009**, submitted.
(45) Backhaus-Ricoult, M.; Adib, K.; St.Clair, T.; Luerssern, B.; Gregoratti, L.; Barinov, A. *Solid State Ionics* **2008**, *179*, 891.

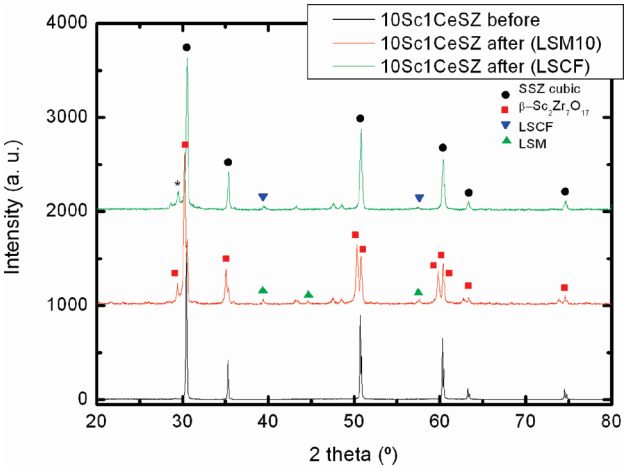

Figure 4. XRD data recorded from the 10Sc1CeSZ electrolyte surface for the LSM10 and LSCF samples after the SOFC-SOE experiments and for a different sample before any electrochemical experiment. *Attributed to phase transformation.

surface region and promotes the direct incorporation of oxygen from the gas into the electrolyte. One explanation for this behavior is that a similar mechanism to that observed in SOFC mode could be occurring in electrolysis mode for the oxygen evolution, explaining the good performance of the LSM/YSZ as a SOEC anode.

Analysis after SOFC-SOE Experiments. AC impedance experiments were also performed after SOFC-SOE experiments. SOFC-SOE data were recorded at different temperatures and gas conditions, and the approximated length of the experiment for each sample was 100 h. In Figure 3, impedance spectra measured at 900 °C for the LSM10 and LSCF samples before and after the SOFC-SOE experiments are presented.

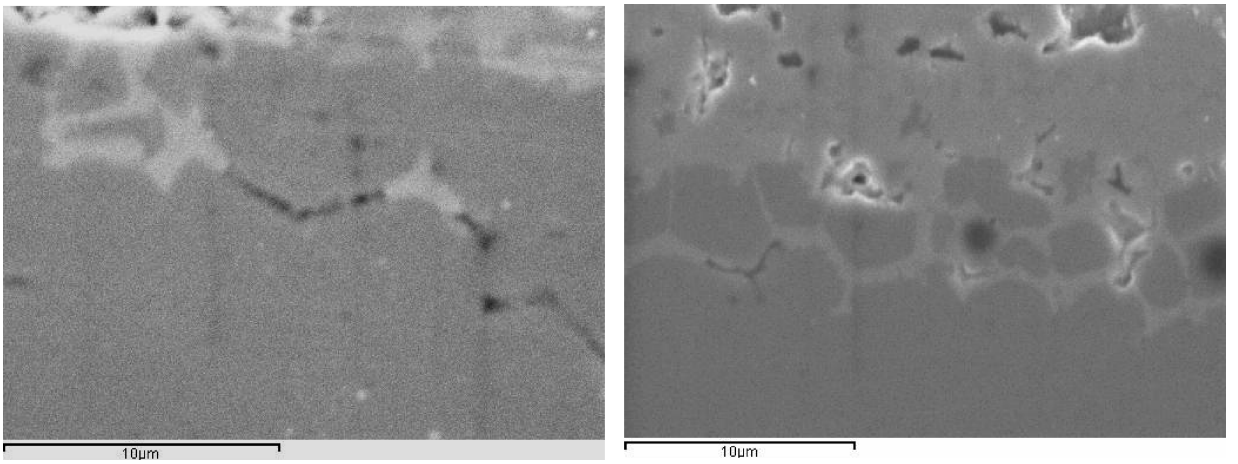

Figure 5. SEM micrographs (polished cross-sections) after SOFC-SOE experiments of the (left) LSM/YSZ-10Sc1CeSZ interface of the LSM10 cell and (right) LSCF-10Sc1CeSZ interface of the LSCF cell.

Equivalent electric circuits were used to fit the electrical data and the parameters obtained from fitting are presented in Table 3. Capacitance values (C) and relaxation frequencies (f) for each contribution are calculated according to eqs 1 and 2, respectively. The obtained values are shown in Table 4, as well as the total area specific resistance ($ASR_{total} = R_e + R_1 + R_2$).

At 900 °C, responses similar to the previously described results measured at 800 °C were obtained. We again assign R_1 as the Ni-YSZ electrode response and R_2 to the oxygen electrode. LSCF results before and after the experiments are almost identical, as seen in all the parameters in both Tables 3 and 4. On the contrary, some changes are observed in the AC impedance of the LSM10 sample. A small increase in R_1 is observed: $0.055 \pm 3\ \Omega\ cm^2$ before to $0.069 \pm 9\ \Omega\ cm^2$ after the experiments, although if we look at the fitting error this difference is almost negligible. Possibly the most remarkable difference is an ~10% increase in the ohmic resistance: $0.107 \pm 3\ \Omega\ cm^2$ to $0.124 \pm 4\ \Omega\ cm^2$. This degradation in the ionic conductivity has been also studied by XRD (Figure 4) and SEM (Figure 5) experiments.

For these XRD experiments, oxygen electrodes were carefully removed by mechanical polishing and then XRD data were collected from the 10Sc1CeSZ electrolyte. As seen in Figure 4, the electrolyte sample before the experiments presents a clear cubic phase (space group $Fm\bar{3}m$). LSM and LSCF peaks with low intensity are observed for the LSM10 and the LSCF samples, respectively. This indicates that the majority of the electrodes have been successfully removed and XRD data were collected near the electrolyte interface. The changes observed in the diffraction patterns are then attributed to degradation of the SSZ electrolyte.

In Figure 4, we also observe that the electrolyte for the LSCF sample is mainly cubic, although a small peak marked with (*) in the figure was observed that could be attributed to a transformation of the cubic stabilized zirconia electrolyte to the ZrO_2 monoclinic phase (space group $P2_1/c$). The LSM10 sample clearly presents a distortion to the rhombohedral β-$Sc_2Zr_7O_{17}$ phase. It is reported that the rhombohedral distortion is a consequence of the presence of oxygen vacancies.[46] These authors also reported that the β-$Sc_2Zr_7O_{17}$ phase is only stable at temperatures below 400 °C and transforms into the cubic phase at higher temperatures. For the sample with the LSM10 electrode, it is conceivable that there is an increase in oxygen vacancy concentration in the electrolyte after operation. Supporting this, we have observed a color change in the samples after the SOFC-SOE experiments that is associated with the reduction of Ce^{4+} to Ce^{3+} in the electrolyte, and as a consequence of this reduction there will be an increase in the oxygen vacancy content, confirming also the rhombohedral distortion in the electrolyte. This β-phase transformation is also the reason for the decrease of the ionic conductivity.

Microstructural studies were also performed after the experiments. In both samples, there is no apparent evolution in the microstructure of both electrodes. If we analyze the region near the oxygen electrode interface in detail, some differences were observed. In Figure 5, we present the microstructure of the LSM10 sample (left) and LSCF sample (right) after the SOFC-SOE experiments in a region near the oxygen electrode/electrolyte interface. We have observed some diffusion of species from the electrode into the 10Sc1CeSZ electrolyte via the grain boundaries in both samples. EDS analysis revealed the presence of only Sc, Zr and La in those particles and formation of small precipitates of $(La, Sc)_2Zr_2O_7$ is suggested. These precipitates have not been detected by XRD. We also consider that they have no effect on the degradation of the conductivity, as we observe them in both samples and we only observe conductivity degradation in the LSM10 sample.

The reason that severe degradation in the electrolyte was observed with the LSM10 in comparison with the LSCF sample is still unclear, but may be associated with reaction between the phases at a level not observed by diffraction techniques. Possibly the increase in the oxygen vacancies is

(46) Spiridonov, F. M.; Popova, L. N.; Popil'skii, R. Ya. *J. Solid State Chem.* **1970**, *2*, 430.

less noticeable for the LSCF sample and it seems to be more stable during operation in SOE mode. This degradation could be avoided by using ceria barrier layers.

4. Conclusions

The performance of LSCF and LSM/YSZ oxygen electrodes for reversible solid oxide fuel cells were presented and discussed. Total ASR values have been found to decrease according to: Pt > LSM12 > LSM10 > LSCF. The impedance response at OCV is characterized by a small arc at high frequencies around 10 kHz assigned to the Ni/YSZ polarization and a larger arc at low frequencies at about 200 Hz associated with the oxygen electrode. High performances in electrolysis mode were measured at 800 °C and using 70% H_2O in the Ni/YSZ and lower polarization resistances were obtained for the LSCF electrode. After operation, degradation in the ionic conductivity was observed. The ~10% increase in the ohmic resistance for the LSM10 sample is consistent with a distortion to the rhombohedral β-$Sc_2Zr_7O_{17}$ phase observed by XRD. Some diffusion of species from the electrode into the 10Sc1CeSZ electrolyte forming deleterious phases, such as $La_2Zr_2O_7$, was observed in both samples, although they do not appear to interfere with the good performance of the cells.

Acknowledgment. We thank UKERC (NERC-TSEC Programme Grant NE/C516169/1) for funding the project.

Note Added after ASAP Publication. Due to a production error, this article published ASAP December 8, 2009 with an incorrect Figure 3 graphic; the corrected version published ASAP December 15, 2009.